ARTICLE NO. 79-4061

Unsteady Pressure Measurements on Rotor Blade Tips with Incidence

Hermann Triebstein*
Deutsche Forschungs- und Versuchsanstalt für Luft- und Raumfahrt E.V., Institut für Aeroelastik, Göttingen, West Germany

Measurements of pressure distributions on a harmonically oscillating rotor blade wing in low subsonic speed are reported. The measurements were carried out in the 3×3 m subsonic wind tunnel of the DFVLR in Göttingen. Pressures were measured at five sections of the wing in such a way that the three-dimensionality of the pressure distribution could be well observed. The flow speed was 45 m/s. The oscillation frequencies were 2, 4, and 6 Hz, with reduced frequencies $\omega^* = \pi f l/V = 0.07$, 0.14, and 0.21. The oscillation amplitudes ranged from $B = 1$-3 deg, and the angles of attack were $\alpha = 0$, 3, 6, 9, and 12 deg. Comparisons with theoretical and experimental results were made. The analytic predictions were found to agree well with the measured data. At the wing tip, however, the agreement was not uniform. A brief description of the test facilities is also presented.

Nomenclature

b	= span
B	= oscillation amplitude in degrees or circular measure
c_{pb}	= amplitude function of pressure coefficient for pitching oscillations
f	= oscillation frequency = $\pi f l/V$
F	= rotor surface
l	= local depth of wing
p	= steady and unsteady pressure
q	= stagnation pressure = $(\rho/2)V^2$
V	= mean velocity
x,y,z	= Cartesian coordinates
α	= angle of attack
Λ	= aspect ratio = b^2/F
ρ	= air density
ξ	= coordinate variable in x direction = x/l

Introduction

NUMEROUS investigations of rotating wings, e.g., helicopter rotors and V/STOL propellers, reveal a distinct relation between turbulent wake of the rotors, their operating and oscillation characteristics, and their noise characteristics. Unsteady aerodynamic effects produced by turbulent wakes retard separation and thus increase lift. As a result of the upstream effects, this increase in lift may, however, be accompanied by effective negative damping in the case of torsional oscillation, leading to substantial torsional deflections of the rotor blades and control difficulties. Such difficulties limit the speed of helicopters. Up-to-date airfoil theory also does not allow a complete solution. Thus, the separation effects require detailed investigation, and sufficient experimental data must be available for the development of a useful theory. The vortex wake of a rotating rotor blade is due to the vortex sheet at the trailing edge and the tip vortex at the end of the span of the rotor. The tip vortex of rectangularly shaped rotor tips is formed by separation of the flow due to the significant pressure gradient at the wing tip. Attempts to decrease this pressure gradient have, at times, greatly reduced the power. It is necessary to develop the edge shape of the rotor tip which prevents concentration of the vortex sheet, leaving the trailing edge and the separation vortex from the side edge.

An attempt was made to determine the unsteady pressure distributions leading to a separation vortex on a nonrotating but oscillating rectangular wing with different end edges. The selected models, flow velocities, and oscillation amplitudes did not correspond completely to those actually occurring in practice; thus, the results are suitable for validation of proposed theories. The pressure distributions were measured by the indirect-method technique. This technique is a refinement of the method already proven for steady measurements. It is based on pressure holes, pressure tubes, and scanning valves with a single pressure gage as the sole measuring element. The specific problems involved here relate to determining the complex transfer function of the transformation system.

Testing Facilities

A. Test Rig

The wing model employed in the experiments projects into the freestream above a base plate extending from the nozzle to the augmenting cone, and is mounted on a solid steel frame. The first measurement section was 60 cm above the base plate, located in the onset flow. No sealing was required between base plate and model to reduce the pressure equalization. The test equipment was designed in such a way to allow for both pitching and flapping oscillations. Any axis could be used as the axis of rotation for pitching oscillations. It was also possible to apply various angles of attack to the wing.

It was possible to easily vary the angles of attack and the amplitudes by means of a hydraulic exciter. The measurements were conducted for oscillation frequencies $f = 2$, 4, and 6 Hz. One advantage of the hydraulic exciter over the electrodynamic exciters previously used was its high-amplitude constancy. The cover plate was mounted above the exciter-cylinder, together with its supply lines and scanning valves, the pressure gages, and the velocity pickups for the amplitude measurements.

B. Test Model

The test model is illustrated schematically in Fig. 1, which also gives the dimensions of the model and the location of the pressure holes. The holes were located at five sections on the wing, with 15 holes on both the pressure and suction surfaces of the rotor. The distribution of the holes on the individual sections in the thickness direction was such that the expected

Received May 30, 1978; revision received Sept. 11, 1978.

Index categories: Aerodynamics; Propeller and Rotor Systems.

*Senior Research Engineer, Institute of Aeroelasticity.

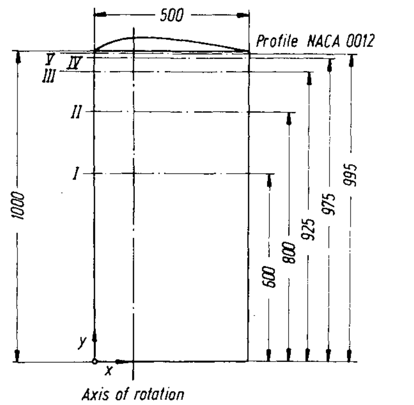

Position of holes, dimensions in mm

Section I + II	x	8	15	30	60	100	150	200	250	300	350	400	425	450	465	480
Section III, IV, V	x	8	13 x 34,571													480

Fig. 1 Test model with indication of the dimensions and position of the pressure holes.

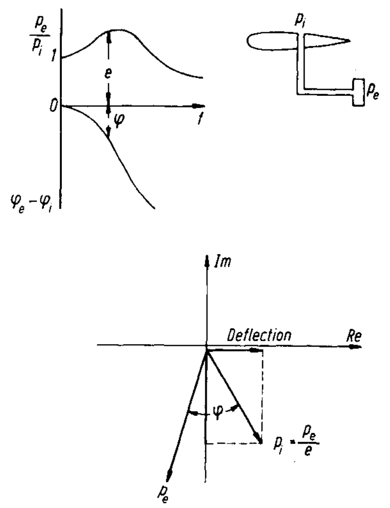

Fig. 2 Basic diagram of pressure transmission in pressure tubes.

pressure distribution peaks were monitored as effectively as possible. The rotor model was a rectangular wing with an aspect ratio $\Lambda = 4$, with an untwisted symmetrical NACA 0012 profile.

The test model was made of a light alloy cast core enclosed in synthetic resin compacted with carbon in a prefabricated mold. Nickel-silver tubes were installed in this synthetic resin layer. After stripping, the tubes were drilled at the required points. The pressures were thus linked via nickel-silver tubes in the model and plastic tubes outside the model to the scanning valves and the pressure gages.

Experimental Principle

All holes in the model for the measurement of unsteady pressures were connected to a central pressure transducer by lines via an electromechanical pressure switch. With the direct method, however, each pressure hole is connected directly to a pressure transducer built into the model. The main advantage of the indirect method used here is its considerably lower cost, by saving on pressure sensors and electronic equipment. There is, however, also the disadvantage connected with a highly complicated transmission function of the pressure waves in the individual pressure tubes to the pressure gages. Thus, the pressure amplitudes to be measured varied in absolute value and phase (Fig. 2), and it was necessary to make corrections by calibration or calculation.

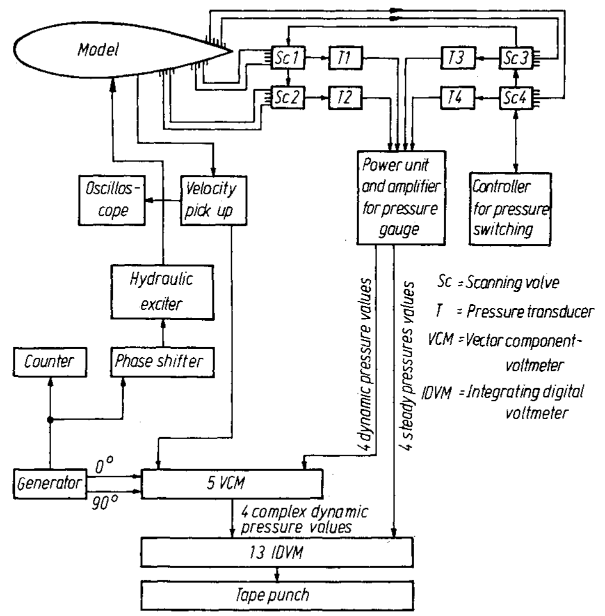

Fig. 3 Block circuit diagram of the electronic measurement equipment.

As indicated in Refs 1, and 2, the pressure transmission function depends on geometric parameters such as radius and length of tubes and volume of the pressure transducers, as well as physical parameters such as oscillation frequency, temperature, steady pressure, and dynamic viscosity of the medium. For incompressible flow in the subsonic wind tunnel of the DFVLR-AVA, the dependence of the transmission function on steady pressure can be neglected. The temperature and dynamic viscosity of the medium remain constant; thus, only the dependence on tube geometry and on oscillation frequency were to be considered.

There are two possible ways of determining the transfer function by means of calibration. On one hand, a pressure transducer may be built directly into the model near a pressure hole for the measurement tube, so that the transfer function can be determined for all tubes of the same geometry at various frequencies. When preparing a test model, however, it is not always possible to make all pressure tubes identical; even if it were possible, dust in the tubes and unforeseeable deformations could lead to quite substantial measuring errors. In our particular case, the transfer function was determined by producing an oscillating pressure with the help of a pressure generator, conducting this pressure through the system of pressure tubes, and then measuring the pressure ahead of the system. A transfer function was thus obtained for each measuring point and tube. In turn, this could be used to correct the measured values of the unsteady pressure.

Electronic Data Control and Processing

The electronic measurement equipment for determining the unsteady pressure distributions is shown as a block diagram in Fig. 3.

It was necessary to measure the following parameters: 1) unsteady pressure distributions on the model from four external pressure transducers, 2×40 and $2 \times 35 = 150$ pressure holes via tubes and scanning valves; 2) transfer function for the pressure tubes at various oscillation frequencies; 3) oscillating amplitudes of the pitching motion; and 4) angles of attack.

A four-phase frequency generator set up the sine wave voltages of the desired frequency ω. A quartz-controlled frequency counter permitted accurate measurement of this frequency and its period. The ac voltage of the generator was passed to the electrodynamic exciter via a phase shifter and a power amplifier in order to produce harmonic pitching oscillations of the model.

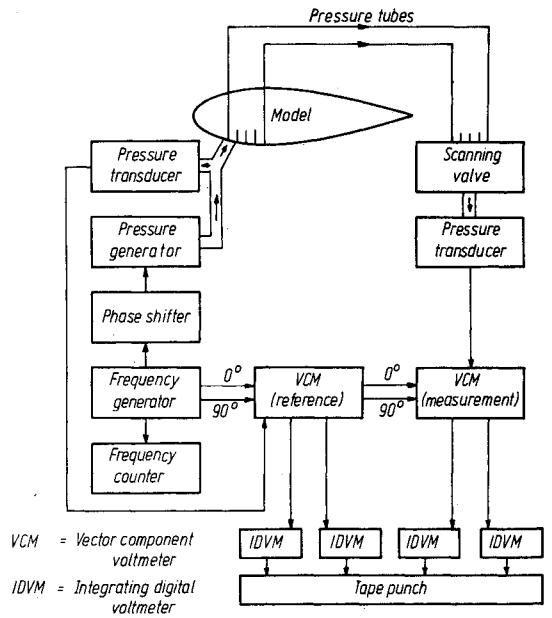

Fig. 4 Block circuit diagram of the calibration measurement.

The four-phase generator voltage was taken as the reference voltage of the two vector component voltmeters. The signal of a velocity pickup on the model was transmitted to the associated vector component voltmeter. The phase shift meter was set in such a way that the real part of the voltage of the velocity transducer was zero. The 0-deg phase of the reference voltage was then in phase with the motion of the model. The oscillation amplitude could be determined from the voltage of the velocity transducer.

The values of the measured pressure of the 150 holes, distributed on the pressure and suction surfaces of the wing, were determined, at the same time, via the four scanning valves and four pressure transducers. The measured values of the vector component voltmeters were ascertained by means of integrating digital voltmeters and recorded on punched strip by means of a puncher.

The method of the calibration measurement is shown in Fig. 4. The pressure generator was controlled from the frequency generator via a phase shifter, which also supplied the reference voltage for the vector component voltmeters. The end sections of the pressure tubes, connected directly to the reference pressure transducer, were then pressed against a pressure measurement hole of the model. If the pressure had built up in the tubes so that the external pressure transducer showed a constant output voltage, then the measurement and punching operations were released immediately. With this method, the pressure amplitude need not remain constant, from one measurement to the measured unsteady pressure determined from the quotient $p_{\text{measurement}}/p_{\text{reference}}$.

Discussion of Typical Results

A. General Remarks

The measurements were carried out on a model of aspect ratio $\Lambda = 4$ with two different end edges. In all the measurements, the freestream velocity was $V = 45$ m/s, and the oscillation frequencies of the pitching oscillations about the quarter-chord were $f = 2$, 4, and 6 Hz. At these oscillation frequencies, the model could be regarded as a rigid one. The reduced frequencies were in the range $\omega^* = \pi f l / V = 0.07\text{-}0.21$. The oscillation amplitudes of the pitching oscillations were in the range $B = 0.92\text{-}2.75$ deg. Dimensionless pressure coefficients were employed to represent the steady pressure distributions as well as the unsteady pressure distributions.

Thus, for the steady values there are:

$$c_p = \frac{p_{u,up}}{q}$$

and for the unsteady values

$$c_{pb} = \frac{p_{u,up}}{q\varphi_N} = c'_{pb} + i\,c''_{pb}$$

Here, p_u is the pressure on the pressure surface, p_{up} is the pressure on the suction surface, and φ_N is the oscillation amplitude for pitching oscillations of the individual measurements.

B. Steady Pressure Distributions for Different Angles of Attack

Figures 5-7 show the steady pressure distributions for a rotor blade tip with and without rounding of the end edges for angles of attack $\alpha = 0$, 6, and 12 deg. These are the two most common shapes of rotors currently in use. The pressure distributions at the various sections were plotted relative to the dimensionless wing depth $\xi = x/l$. The sections were selected in a manner such that the center section yields virtually two-dimensional results without being affected by the pressure equalization at the base plate. The other four sections were located in such a manner that the pressure distributions at the pressure peak could be determined as efficiently as possible. The steady pressure distributions are needed when evaluating unsteady theoretical results, especially for the transition from the oscillating thin plate to thick profiles. The steady pressure distributions were determined by suitable integration of the pressure values on the oscillating wing. They were measured at the same time as the unsteady values.

The pressure distributions for angle of attack $\alpha = 0$ deg were not affected by the different rotor blade shapes. As expected, in the case of a symmetrical profile, the values on the pressure and suction faces are equal. Slight deviations, especially at the leading edge of the profiles, were due to insufficient integration time. The three-dimensionality of the flow is clearly discernible in the results obtained for the individual sections.

As expected, the lift area increases with angle of attack. On the basis of the three-dimensional flow, this area is reduced for the outer sections. It is interesting to note that, for the outermost section, i.e., right at the end of the rotor blade, a pressure peak arises on the suction face which increases with angle of attack. A vortex is formed on the rotor by the pressure equalization. The intensity of the vortex thus formed is a function of the angle of attack and the shape of the outer edge. At higher angles of attack the vortex breaks down. The pressure peak formation, reduced in this manner, is less intensive than the pressure of rounded outer edges. The pressure pattern and thus the formation of the tip vortex can be clearly affected by the design of the end edges. The optimum shape remains to be determined. The effect of the pressure equalization at the rotor end on the pressure pattern is more pronounced in the case of a straight edge in the direction of the wing root than with a rounded edge, especially at larger angles of attack.

C. Unsteady Pressure Distribution for Different Angles of Attack and Frequencies

As for the case of measurements of steady pressure distribution, the measurements of unsteady pressure distribution on the two configurations of rotor ends described were carried out for angles of attack $\alpha = 0$, 3, 6, 9, and 12 deg, and for the oscillation frequencies $f = 2$, 4, and 6 Hz in the five sections each containing 15 holes on each face. The pitching oscillations occurred near the quarter-chord of the rotor blade. The pitching frequencies were in the range of rotation frequency of the rotor, whereas the amplitudes did not reach

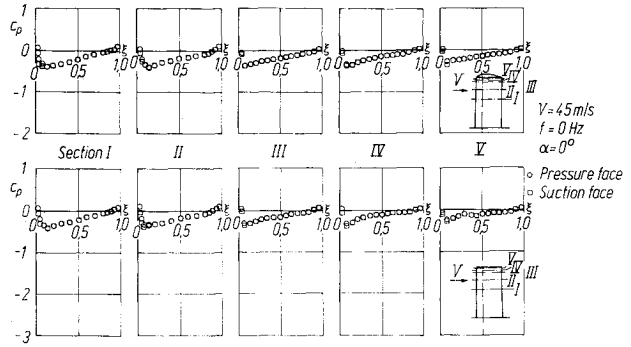

Fig. 5 Steady pressure distribution on rotor blades with and without end edge rounding, $\alpha = 0$ deg.

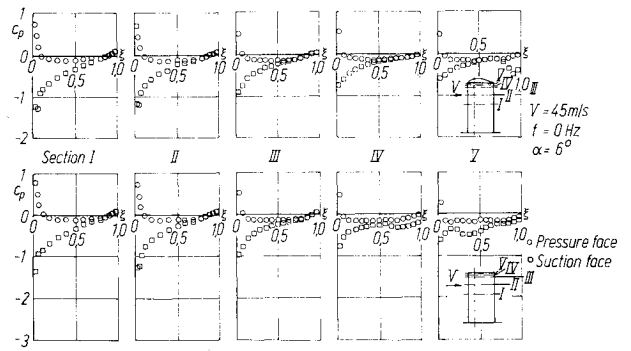

Fig. 6 Steady pressure distribution on rotor blades with and without end edge rounding, $\alpha = 6$ deg.

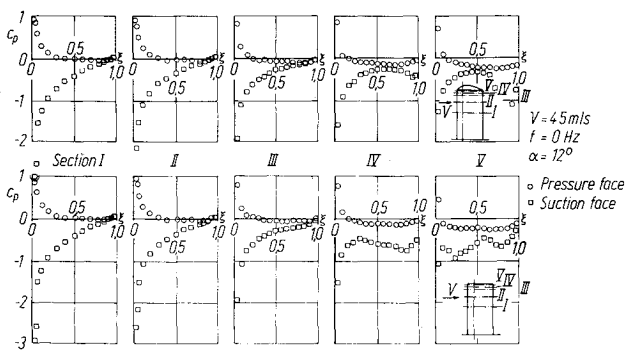

Fig. 7 Steady pressure distribution on rotor blades with and without end edge rounding, $\alpha = 12$ deg.

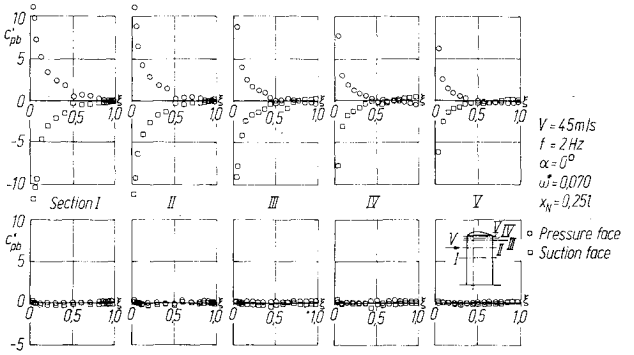

Fig. 8 Real and imaginary parts of the unsteady pressure distribution in the case of pitching oscillations around the quarter-chord on a rotor blade with end edge rounding.

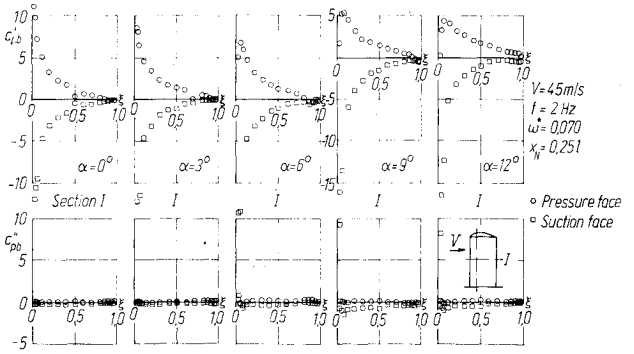

Fig. 9 Real and imaginary parts of the unsteady pressure distribution in the case of pitching oscillations around the quarter-chord on a rotor blade with end edge rounding at different angles of attack, Sec. I.

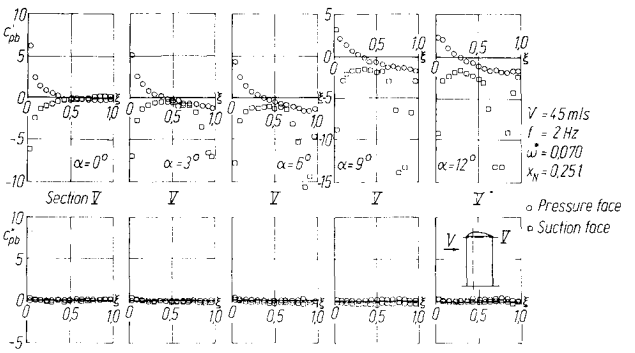

Fig. 10 Real and imaginary parts of the unsteady pressure distribution in the case of pitching oscillations around the quarter-chord on a rotor blade with end edge rounding for different angles of attack, Sec. V.

the angles of attack actually occurring in practice. In the enclosed figures, the unsteady pressure was split up into real and imaginary parts and plotted against the dimensionless wing depth ξ for the individual sections, on both the pressure and the suction surfaces.

Figure 8 shows the unsteady pressure distribution for the oscillation frequency $f = 2$ Hz and an angle of attack $\alpha = 0$ deg. A symmetrical pattern of pressure distributions was found in the real and imaginary parts of both the pressure and the suction surfaces. This applied also to higher frequencies. The three-dimensionality of the flow was also easily discernible from the unsteady pressure distributions in Secs. I to V. As the values of Sec. II were the same as those of Sec. I, these sections can be regarded as having two-dimensional flow.

The symmetry of pressure patterns is, of course, greatly altered in the case of pressure distributions with increasing angles of attack (Fig. 9). In the real part, the pressure peaks at the pressure surface decrease and the suction peaks increase for increasing angles of attack. The pressure peak of the suction surface at the rotor blade end also becomes more pronounced for increasing angles of attack, and moves toward the leading edge of the airfoil (Fig. 10). This applies only to the real part, the imaginary part was completely unaffected. The reduced pressure peaks were due to increased local velocities. The "piping vortex," forming at the ends, prevents pressure equalization, until it breaks down.

A definite dependence on angle of attack and on oscillation frequency is apparent. This can be recognized by the results for $f = 2$, 4, and 6 Hz and $\alpha = 3$, 6, 9, and 12 deg. Just as with the frequency $f = 2$ Hz, the unsteady pressure at the rotor blade end on the pressure surface becomes less noticeable on increase of angle of attack at frequencies $f = 4$ and 6 Hz; whereas the suction surface is greatly affected, as was mentioned earlier. In the case of $\alpha = 3$ deg, the vortex seems to break down behind the airfoil in such a manner that the Kutta condition is not fulfilled. At higher frequencies, the real part values shift, and thus the phase angle between the motion and the pressure increases.

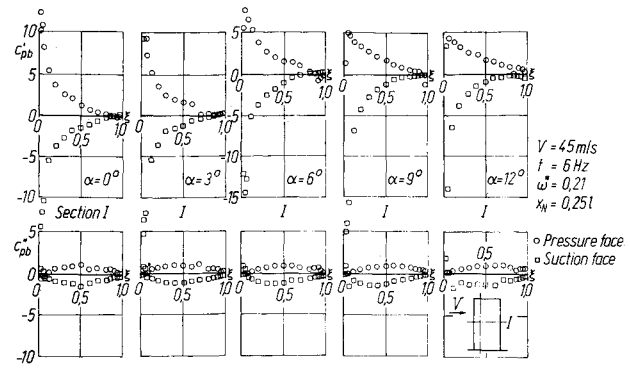

Fig. 11 Real and imaginary parts of unsteady pressure distribution in the case of pitching oscillations around the quarter-chord on a rotor blade without end edge rounding for different angles of attack, Sec. I.

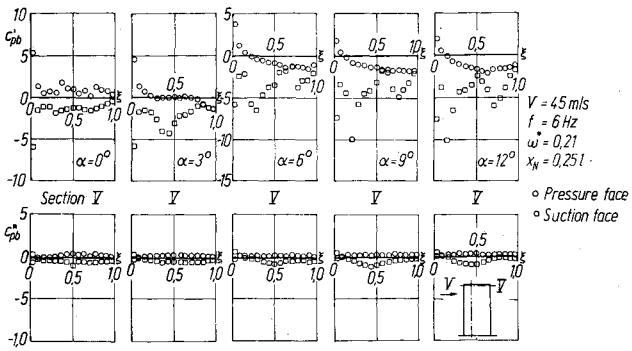

Fig. 12 Real and imaginary parts of unsteady pressure distribution in the case of pitching oscillations around the quarter-chord on a rotor blade without end edge rounding for different angles of attack, Sec. V.

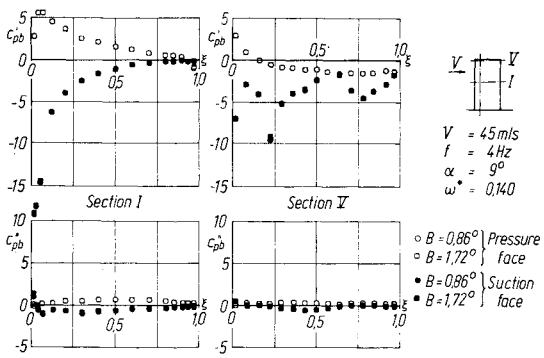

Fig. 13 Influence of oscillation amplitude on the unsteady pressure distribution in the case of pitching oscillations around the quarter-chord of a rotor blade.

Figures 11 and 12 show the unsteady pressure distributions at Secs. I and V for the rotor blade tip without rounding, for the angles of attack $\alpha = 0$, 3, 6, 9, and 12 deg, and the frequency $f = 6$ Hz. These results agree for other frequencies too; satisfactorily with those at the rotor blade tip with rounding in Secs. I-III. Major differences are evident, however, in Sec. IV and in particular Sec. V. Here, a suction pressure peak is found at the leading edge of the airfoil at low angles of attack. At increased angles of attack, a further suction peak forms on the trailing edge of the blade. This does not seem to be clearly dependent on the frequency.

Figure 13 shows the real and imaginary parts of the unsteady pressure distribution for Secs. I and V in the case of the rotor blade tip without rounding. The measurements were

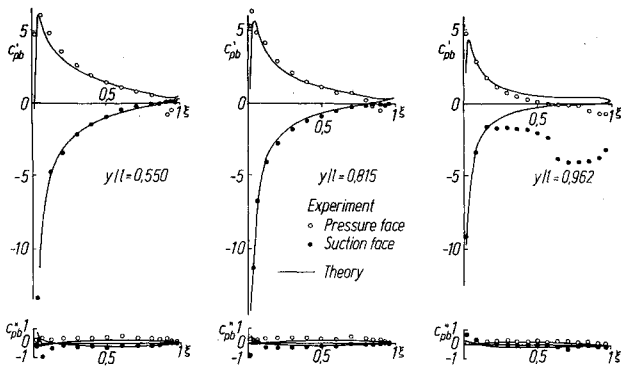

Fig. 14 Theoretical and experimental results of unsteady pressure distribution in the case of pitching oscillations around the quarter-chord on a rotor blade without end edge rounding.

carried out for different oscillation amplitudes and then plotted. As the unsteady values were normed to a single amplitude, the values had to conform, subject to a linear dependence on the amplitude. This applies also to the different frequencies and angles of attack and to the rounded tip, including Sec. V. Any deviations from this were due to measurement errors. Figure 14 shows a comparison between theoretical[3] and experimental results. A good agreement in Secs. I and III is evident, but not for Sec. V, especially on the suction surface.

Conclusions

The measurement method and the experimental configuration for measuring unsteady pressure distributions in the 3 × 3 m wind tunnel of the DFVLR-AVA were presented. The measurements were carried out for frequencies $f = 2$, 4, and 6 Hz in the case of pitching oscillations around the quarter-chord, for angles of attack $\alpha = 0$, 3, 6, 9, and 12 deg, and amplitudes $B = 0.92$-2.75 deg. Special preparations were made for the pressure distributions at the very end of the wing. The steady and unsteady distributions on a nonrotating but oscillating rectangular wing with different end edges could be determined. The selected end edges correspond to the usual present-day designs of helicopter rotors. Various steady and unsteady results were also given. The oscillation frequencies were within the operating range of blades. The mean flow velocity and oscillation amplitudes do not correspond to the ones found in practice. These limitations were due to factors relating to the wind tunnel itself and the strength of the test model. The results are suitable for validating vortex theories.

The results confirm previous knowledge concerning end-edge vortices. The intensity of the edge vortex is a function of the angle of attack, the oscillation frequency, and, in particular, the configuration of the end edges. Comparisons with theoretical results from airfoil theory and experimental results show good agreement. At the tip, however, the agreement starts to deteriorate.

References

[1] Bergh, H. and Tijdeman, H., "Theoretical and Experimental Results for the Dynamic Response of Pressure Measuring Systems," NLR Report TR-F.238, 1965.

[2] Triebstein, H., "Entwicklung und Errichtung eines Versuchsstandes zur Messung instationärer Druckverteilungen an schwingenden Modellen im Transsonischen Windkanal der AVA. Part III: Theoretische und experimentelle Untersuchungen des dynamischen Verhaltens von Druckübertragungsleitungen," AVA Report 68 J04, 1968.

[3] Geissler, W., "Calcuation of Unsteady Airloads on Oscillating Three-Dimensional Wing and Bodies," AGARD CP-227, Paper No. 5, 1977.